Double spin-flip approach within equation-of-motion coupled cluster and configuration interaction formalisms: Theory, implementation, and examples

David Casanova,[1,a)] Lyudmila V. Slipchenko,[2] Anna I. Krylov,[3] and Martin Head-Gordon[1]
[1]*Department of Chemistry, University of California, Berkeley, California 94720, USA*
[2]*Department of Chemistry, Purdue University, West Lafayette, Indiana 47907-2084, USA*
[3]*Department of Chemistry, University of Southern California, Los Angeles, California 90089-0482, USA*

(Received 22 September 2008; accepted 15 December 2008; published online 27 January 2009)

The spin-flip (SF) approach is extended to excitations that flip the spin of two electrons to describe multiconfigurational $M_s=0$ wave functions via high spin quintet references. Equations and implementation of the double SF (2SF) approach within equation-of-motion coupled-cluster (EOM-CC) and configuration interaction (CI) formalisms are presented. The numerical performance of the resulting EOM-2SF-CC and 2SF-CI models is demonstrated by calculations of symmetric dissociation of O–H bonds in water, electronic states of linear H_4, double CC bond-breaking in ethylene, and low-lying states of trimethylenemethyl diradical and 2,4-didehydrometaxylylene tetraradical. The results of active-space variants of 2SF are very close to the more computationally expensive full-space counterparts. An efficient implementation of the active-space approximation of the 2SF-configuration interaction doubles (CID) model termed 2SF-configuration interaction singles (CIS) is also reported. The scaling of 2SF-CIS is only N^4, which allows applications to relatively large molecules. © *2009 American Institute of Physics*. [DOI: 10.1063/1.3066652]

I. INTRODUCTION

Electronic degeneracies and quasidegeneracies often encountered in open shell species (e.g., transition metals, polyradicals, and molecules with broken bonds) lead to multiconfigurational wave functions that present a challenge to *ab initio* methods. Traditionally, multiconfigurational wave functions are described using a multireference formalism, starting with the complete active space self-consistent field (CASSCF),[1,2] which is further augmented by multireference perturbation theory (MRPT), multireference configuration interaction (MRCI), or multireference coupled-cluster (MRCC) corrections.[3–6] Similar ideas involving configuration selection through the active space have also been explored within the coupled-cluster formalism.[7–9]

An alternative strategy that has the simplicity of the single reference formalism is to describe complex multiconfigurational wave functions as excitations from a judiciously chosen well-behaved reference state. By combining different type of references and excitation operators, different groups of target states can be described.[10] For example, open shell excited states can be described as single electron-conserving excitations from a closed shell reference; doublets can be reached by ionizing or electron attaching excitations, and so on.

Most examples of such multistate single-reference approach to multiconfigurational wave functions belong to the equation-of-motion coupled-cluster (EOM-CC) family of methods,[11–19] closely related linear response coupled-cluster (LR-CC),[20–23] or symmetry-adapted cluster configuration interaction (SAC-CI) methods;[24–26] however, there are also examples of CI based models, e.g., the familiar configuration interaction singles[24] (CIS) or time-dependent density functional theory[27–29] (TD-DFT) methods.

The focus of this work is on the spin-flip (SF) approach,[30,31] in which multiconfigurational low spin states are described as spin-flipping excitations from a well-behaved high spin reference. For example, diradical-type wave functions of the "two electrons in two orbitals" type can be generated from the $|\alpha\alpha\rangle$ reference state, whereas triradical states ("three electrons in three orbitals") can be described as spin-flipping excitations from the $|\alpha\alpha\alpha\rangle$ quartet reference

$$^{s,t}\Psi^{M_s=0} = \hat{R}^{\Delta M_s=-1}\,{}^{t}\Psi^{M_s=+1}, \tag{1}$$

$$^{d,q}\Psi^{M_s=1/2} = \hat{R}^{\Delta M_s=-1}\,{}^{q}\Psi^{M_s=+3/2}, \tag{2}$$

where $^{t}\Psi^{M_s=+1}$ and $^{q}\Psi^{M_s=+3/2}$ are the high spin components of the reference triplet and quartet states, respectively, $^{s,t}\Psi^{M_s=0}$ denotes the target open and closed shell singlet and triplet states, and $^{d,q}\Psi^{M_s=1/2}$ denotes the target low spin doublets and quartets. $\hat{R}^{\Delta M_s=-1}$ is an excitation operator that flips the spin of an electron,

$$\hat{R}^{\Delta M_s=-1} = \sum_{i\bar{a}} r_i^{\bar{a}} a_{\bar{a}}^{\dagger} a_i + \cdots, \tag{3}$$

where a bar is used to distinguish β spin orbitals. Indices $i,j,k,\ldots$ and $a,b,c,\ldots$ denote occupied and virtual spin orbitals with respect to the reference determinant Φ_0, respectively.

[a)]Electronic mail: davidcasanova@berkeley.edu.

The SF idea has been implemented within EOM-CC,[15,30,32] TD-DFT,[33,34] as well as CI (Refs. 35–38) methods. Although the simplest model (SF-CIS) does not include dynamical correlation, it nonetheless provides qualitatively correct zero order wave functions that can be improved perturbatively.[35] The explicit inclusion of higher excitations as in EOM-SF-CCSD or SF-CISD improves the accuracy considerably, and the inclusion of triple excitations[32,39] brings the error bars below chemical accuracy (1 kcal/mol).

All previous implementations of SF were based on *single* spin-flip $\hat{R}^{\Delta M_s=-1}$ operators, which restricted applications of the method to systems in which strong nondynamical correlations arise from a small HOMO-LUMO gap involving nondegenerate orbitals, e.g., single bond-breaking,[40] diradicals,[41] and triradicals.[42] Tackling more extensive degeneracies, e.g., double bond-breaking, tetraradicals, etc., requires a higher multiplicity reference and *multiple* spin-flips, i.e., $\hat{R}^{\Delta M_s=-2}$ operators acting on high spin quintet references. Towards this goal, we introduce a double spin-flip (2SF) family of methods in this paper. We present working implementations within EOM-CC and CI formalisms, and explore cost-efficient approximations. The primary focus of the paper is on the simplest 2SF model (2SF-CIS), which is a minimal qualitatively correct 2SF wave function, that is applicable to large systems. The capabilities and the performance of 2SF are demonstrated by the following examples: stretching of H_4 molecule, double bond-breaking in water and ethylene, and the electronic excitations in the trimethylenemethyl (TMM) diradical and 2,4-didehydrometaxylylene (DDMX) tetraradical.

II. THEORY

By virtue of the two electron character of double spin-flip operators, the lowest level of a 2SF model in the CI hierarchy is 2SF-configuration interaction doubles (CID), in which the target singlet, triplet, and quintet wave functions ${}^{s,t,q}\Psi^{M_s=0}$ are described as linear combination of all doubly excited determinants that include double spin-flip from the high spin quintet reference determinant $\Phi_0^{M_s=2}$,

$$ {}^{s,t,q}\Psi^{M_s=0} = \hat{R}_2^{\Delta M_s=-2}\Phi_0^{M_s=2} = \frac{1}{4}\sum_{ij\bar{a}\bar{b}} r_{ij}^{\bar{a}\bar{b}}\Phi_{ij}^{\bar{a}\bar{b}}, \tag{4}$$

where the coefficients of the expansion $r_{ij}^{\bar{a}\bar{b}}$ are found by diagonalizing the Hamiltonian in the basis of all target $M_s=0$ $\Phi_{ij}^{\bar{a}\bar{b}}$ determinants. The size of the expansion is proportional to O^2V^2, where O and V denote the number of occupied and unoccupied molecular orbitals, respectively. Further on, the following notations will be used to refer to different orbital subspaces: S for singly occupied, N for total number of molecular orbitals (MOs), and X for auxiliary basis functions.

From the computational point of view, the memory, disk, and CPU demands of 2SF-CID are similar to a non-spin-flip CID model, which scales as N^6 and the storage requirements are proportional to O^2V^2.

Based on the analogy with the single SF hierarchy of methods, one may expect that the inclusion of triple excitations (i.e., within 2SF-CIDT) is necessary to match the numeric accuracy of SF-CISD. On the other hand, the full set of double excitations is much larger than the set of singles, and includes determinants that are formally excited with respect to the leading 2SF configurations, which might result in a better performance of 2SF-CID, as compared to SF-CIS. We will address this question by comparing SF and 2SF methods. Differences between 2SF-CID and 2SF-CIDT will help to understand the role of triples in such models.

We also implemented 2SF variants of EOM-CC, in which the target wave functions are described as $\Delta M_s=-2$ excitations from the high spin CCSD reference wave function,

$$ {}^{s,t,q}\Psi^{M_s=0} = (\hat{R}_2^{\Delta M_s=-2} + \hat{R}_3^{\Delta M_s=-2})e^{\hat{T}_1+\hat{T}_2}\Phi_0^{M_s=2}, \tag{5}$$

where $\hat{T}_1$ and $\hat{T}_2$ are the high spin reference state CC amplitudes, and the form of the $\hat{R}_{2,3}$ operators is the same as their 2SF-CI counterparts. Including only double EOM excitations ($\hat{R}_2$) gives rise to the EOM-2SF-CCSD or EOM-2SF-CC(2,2) model, whereas including both $\hat{R}_2$ and $\hat{R}_3$ defines EOM-2SF-CC(2,3). For brevity, we will refer to these EOM-2SF-CC models as 2SF-CCSD and 2SF-CC(2,3), respectively.

Similarly to CI, the coefficients of the EOM operators $\hat{R}$ are found by diagonalizing the similarity transformed Hamiltonian in the basis of all doubly and triply excited 2SF determinants. Thus, the computational scalings of 2SF-CCSD and 2SF-CC(2,3) are the same as 2SF-CID and 2SF-CIDT, respectively. The similarity transformation, which introduces additional correlation in the EOM eigen-problem, results in the improved accuracy of EOM-CC methods relative to the corresponding CI models. For non-SF models, the similarity transformation also ensures size intensivity of EOM results. However, the SF-CI models are already size intensive, and thus less dramatic difference in numeric performance between EOM and CI models has been observed.[35,37] By comparing 2SF-CI and 2SF-CC results, we will assess the importance of the similarity transformation for the 2SF methods.

The computational cost of 2SF models with triple excitations, which scales as N^8, limits their application to very small systems. The scaling can be reduced by restricting the triples to a semi-internal subset, as in the active space variants of the EOM-CC(2,3) and EOM-CCSDT methods.[32,43] The semi-internal subset is defined such that at least one electron is excited within singly occupied subspace, which thereby includes all triply excited determinants that correlate the leading electronic configurations of the target 2SF wave functions,

$$ \hat{r}_3 = \frac{1}{36}\sum_{ijKAbc} r_{ijK}^{Abc} a_A^\dagger a_b^\dagger a_c^\dagger a_K a_j a_i, \tag{6}$$

where the capital letter indexes denote orbitals from the active space. We will refer to the 2SF models with the restricted set of triple excitations as 2SF-CC$(2,\tilde{3})$ and 2SF-CID$\tilde{\text{T}}$. Slipchenko and Krylov reported[32] encouraging results for the EOM-CC$(2,\tilde{3})$ model, e.g., they observed errors of the order of 0.01 and 0.1 eV for singly and doubly

excited states, respectively. The number of the resulting triple excitations is $S^2O^2V^2$, which allows an implementation that scales similarly to 2SF-CID.

A similar active space idea can be used to reduce the computational scaling of 2SF-CID to that of the CIS method. By restricting double excitations to the set that includes at least one excitation within the singly occupied subspace, we arrive at a model that we will call 2SF-CIS (or, in the notation used above, it would be 2SF-CI$\tilde{\text{D}}$),

$$\Psi_{\text{2SF-CIS}} = \frac{1}{4}\sum_{i\bar{a}J\bar{B}} r_{iJ}^{\bar{a}\bar{B}}\Phi_{iJ}^{\bar{a}\bar{B}} = \frac{1}{4}\sum_{i\bar{a}s\bar{s}'} r_{is}^{\bar{a}\bar{s}'}\Phi_{is}^{\bar{a}\bar{s}'}, \tag{7}$$

where s and s' denote orbitals from S. The 2SF-CIS wave function retains all the configurations with no less than three and no more than five electrons in the singly occupied subspace. The size of the 2SF-CIS expansion is proportional to OVS^2, which represents a dramatic reduction relative to 2SF-CID. The computational scaling of 2SF-CIS is therefore similar to CIS: formally N^4 per state in the MO basis or even less when contractions are performed in the atomic orbital (AO) basis [as is the case for CIS (Ref. 44)].

A. Size consistency

At this point, a cautious reader could be concerned about the possible violation of size consistency by 2SF-CI, an important and well known deficiency of the truncated CI models leading to degradation of the final state energies with the system size.[45] Whereas non-spin-flip CI is only size consistent (or, more rigorously, size intensive) within the singly excited expansion of the wave function, for the SF methods this property is fulfilled up to the inclusion of doubly excited determinants.[35,37] Using the same arguments as in Ref. 37, it is straightforward to show that 2SF-CI truncations are size intensive up to the inclusion of triple excitations: 2SF-CIDT. More generally, the size intensivity of a multiple SF-CI method is preserved if it contains no more than a single non-spin-flip excitation. A detailed proof and discussion of size intensivity in spin-flip methods are presented in the Appendix.

B. Implementation

2SF-CID, 2SF-CIDT, 2SF-CCSD, and 2SF-CC(2,3) models are implemented within the coupled-cluster module of the Q-CHEM electronic structure package[46] in the spin orbital representation, as described in Refs. 15, 32, and 47. 2SF-CIS is implemented in a much more efficient fashion, i.e., in addition to its intrinsically lower scaling, the atomic orbital representation[44] is employed with the resolution-of-the-identity (RI) approach,[48,53] as discussed below.

The core of the 2SF-CIS algorithm is the iterative Davidson procedure,[54] in which the Hamiltonian matrix is diagonalized in the basis of 2SF-CIS determinants $\{\Phi_K\}$,

$$\boldsymbol{A}\boldsymbol{r}(k) = \omega_k \boldsymbol{r}(k), \tag{8}$$

$$A_{LK} \equiv \langle \Phi_L | H - E_0 | \Phi_K \rangle, \tag{9}$$

where ω_k and $\mathbf{r}(k)$ are the excitation energy and the amplitude vector for state k, respectively, and E_0 is the reference energy. Since the set $\{\Phi_K\}$ of 2SF-CIS determinants is vastly smaller than that of 2SF-CID, the disk storage requirements of the wave function amplitudes $\mathbf{r}(k)$ are only proportional to OV rather than O^2V^2.

Calculation of σ-vectors for the Davidson procedure, i.e., the contraction of the left side of Eq. (8), requires four different kinds of four center integrals involving α-S and/or β-S orbitals denoted as s and s',

$$\begin{aligned} &I^{\bar{a}s\bar{b}\bar{s}'} = (\bar{a}s \,\|\, \bar{b}\bar{s}'); \quad I_{isks'} = (is \,\|\, ks'); \\ &I_{ik}^{\bar{a}s} = (ki|\bar{a}s); \quad I_{is}^{\bar{a}\bar{b}} = (is|\bar{a}\bar{b}). \end{aligned} \tag{10}$$

Since the dimension of orbital subspace S is fixed (and equals four for a high spin quintet reference), the storage space requirements of the $\boldsymbol{I}$ matrices of Eq. (10) scales as third order (OV^2S) of the system size. For moderately large systems, the $\boldsymbol{I}$ matrices can be precomputed prior to the Davidson procedure and stored on disk. The highest scaling step in the contraction of $\boldsymbol{I}$ with the amplitude vectors $\boldsymbol{r}(k)$ scales as OV^2. The only contribution to the σ-vector calculation that cannot be performed using the integrals defined in Eq. (10) contains the four center integrals with all the orbitals outside the S space,

$$(Ar)_{is}^{\bar{a}\bar{s}'} = -\sum_{j\bar{b}} (ij|\bar{a}\bar{b}) r_{js}^{\bar{b}\bar{s}'}. \tag{11}$$

This contraction can be implemented using the following pseudodensity and the associated exchange matrices,

$$P_{\mu\nu}^{s\bar{s}'} \equiv \sum_{i\bar{a}} C_{\mu\bar{a}} C_{\nu i} r_{is}^{\bar{a}\bar{s}'}, \tag{12}$$

$$K_{\sigma\lambda}^{s\bar{s}'} \equiv \sum_{\mu\nu} (\mu\sigma|\nu\lambda) P_{\mu\nu}^{s\bar{s}'}, \tag{13}$$

where $\boldsymbol{C}$ is the MO coefficient matrix. An alternative implementation employs the RI approximation[48–53] using the following $\boldsymbol{B}$ matrices:

$$B_{ij}^{Q} = \sum_{P} (ij|P)(P|Q)^{-1/2}, \tag{14}$$

$$B_{\bar{a}\bar{b}}^{Q} = \sum_{P} (\bar{a}\bar{b}|P)(P|Q)^{-1/2}. \tag{15}$$

The storage of the above matrices is proportional to $(O^2+V^2)X$. Within the RI approximation, the cost of the contraction of Eq. (11) grows as OV^2S^2X and constitutes the most expensive step of the iterative procedure.

Either implemented using the pseudodensity matrices or within RI scheme, 2SF-CIS represents a very substantial reduction of the computational demands with respect to 2SF-CID. The 2SF-CIS results presented in this paper have been obtained using the RI approximation.

C. Spin expectation value in 2SF-CIS

A potentially problematic feature of the n-SF methods is their spin incompleteness, which may lead to spin contamination of the target wave functions.[30,37,38] As the simplest member of the 2SF family, the 2SF-CIS method is probably the most vulnerable to this problem. Therefore the computation of $\langle \hat{S}^2 \rangle$ provides an important gauge of the quality and even the validity of the target wave functions.

The computation of the spin expectation value of the simplest 2SF-CI method is carried out using the $\hat{S}^2$ operator in the Löwdin representation. For a high spin quintet reference, it assumes the following form:

$$\langle \hat{S}^2 \rangle = N_\beta + 2 + S_U^2 + S_T^2 + S_S^2, \tag{16}$$

where N_β is the number of β-electrons, S_U^2 is the squared norm of matrix $\boldsymbol{U}$ defined as

$$\mathbf{U} = \mathbf{U}^{\mathrm{SS}} - \mathbf{U}^{\mathrm{OS}} - \mathbf{U}^{\mathrm{SV}} + \mathbf{U}^{\mathrm{OV}}, \tag{17}$$

and the individual blocks are

$$U^{\mathrm{SS}}_{s\bar{s}'} = \sum_{i\bar{a}} r^{\bar{a}s'}_{is} S_{i\bar{a}}, \tag{18}$$

$$U^{\mathrm{OV}}_{i\bar{a}} = \sum_{s\bar{s}'} r^{\bar{a}s'}_{is} S_{s\bar{s}'}, \tag{19}$$

$$U^{\mathrm{OS}}_{i\bar{s}'} = \sum_{s\bar{a}} r^{\bar{a}s'}_{is} S_{s\bar{a}}, \tag{20}$$

$$U^{\mathrm{SV}}_{s\bar{a}} = \sum_{i\bar{s}'} r^{\bar{a}s'}_{is} S_{i\bar{s}'}, \tag{21}$$

where $S_{i\bar{a}}$ is the spatial overlap between the i_α and a_β orbitals. S_T^2 contains the contractions between $\boldsymbol{T}$ matrices [Eqs. (23)] and the CI amplitudes ($\boldsymbol{r}$),

$$S_T^2 = \sum_{\Omega} r^{\bar{a}s'}_{is} [T^{\alpha}_{ij} r^{\bar{a}s'}_{js} + T^{\alpha}_{ss''} r^{\bar{a}s'}_{is''} - T^{\beta}_{\bar{a}\bar{b}} r^{\bar{b}s'}_{is} - T^{\beta}_{\bar{s}'\bar{s}''} r^{\bar{a}s''}_{is} + 2(T^{\beta}_{\bar{a}\bar{s}''} r^{\bar{s}'\bar{s}''}_{is} - T^{\alpha}_{is''} r^{\bar{a}s'}_{ss''})] \tag{22}$$

where Ω refers to the sum over all indices and $\boldsymbol{T}$ matrices are defined as

$$T^{\alpha}_{ij} = \sum_{\bar{k}} S_{i\bar{k}} S_{j\bar{k}}, \quad T^{\beta}_{\bar{a}\bar{b}} = \sum_{k} S_{\bar{a}k} S_{\bar{b}k}. \tag{23}$$

Finally, the S_S^2 term in Eq. (16) corresponds to the trace of $\boldsymbol{T}^\alpha$.

Calculation of $\langle \hat{S}^2 \rangle$ for the rest of 2SF-CI and 2SF-CC methods can be implemented using one and two particle EOM density matrices, as in Ref. 55.

III. RESULTS AND DISCUSSION

A. Computational details

Potential energy surface (PES) scans along the coordinate for symmetric double bond-breaking in water were computed using the cc-pVDZ basis[56] with pure angular momentum d-functions. The molecular angle was fixed at 109.57°, and the geometries were restricted to C_{2v}. H_4 calculations employed the 6-31G** basis.[57] The PES scans along double CC bond-breaking in ethylene were computed using the 6-31G* basis. All other degrees of freedom were optimized along the scan at the B3LYP/6-31G* level. For large interatomic distances ($r_{CC} > 1.7$ Å), the HCH angle has been fixed at the $r_{CC} = 1.70$ Å optimized value of 116.2°. All electrons were correlated in 2SF calculations of double bond-breaking curves. These calculations employed the high spin UHF reference.

For TMM, two bases were used: the small 6-31G* (Ref. 57) and the larger cc-pVTZ (Ref. 56) basis sets. Equilibrium geometries (see supporting information[58]) and zero point energies (ZPEs) were taken from Ref. 41. Both restricted and unrestricted Hartree–Fock references were used in 2SF calculations. The four lowest occupied orbitals were kept frozen in correlated calculations.

The 6-31G* basis[57] was used in DDMX calculations. Vertical state ordering was computed at the B3LYP/cc-pVTZ equilibrium geometry of the $^5B_2$ quintet state.[58] Eight lowest occupied (core) and eight highest virtual orbitals were kept frozen in 2SF calculations of DDMX. As in the previous examples, the active space was chosen to include four singly occupied orbitals. To benchmark the 2SF results, CASSCF, and MRPT calculations were performed at the same geometry and basis set, with ten electrons in ten orbitals (all singly occupied orbitals plus six benzene-ring π orbitals) active space. Two states of each multiplicity and symmetry were optimized simultaneously in the root-averaging procedure. MRPT calculations employed second-order multiconfigurational quasidegenerate perturbation theory (MCQDPT).[59,60] These calculations were performed with the GAMESS electronic structure package.[61] A four-orbital-four-electron active space was used in MRCI calculations, which were performed with MOLPRO.[62]

The relevant molecular structures and total energies are available as EPAPS supplementary material.

B. Symmetric stretching of water

The symmetric stretching of water is an example of simultaneous breaking of two single bonds. We compare 2SF energy scans against FCI results, as well as CASSCF and CCSDT from Ref. 63.

A suitable 2SF quintet reference configuration for the symmetric dissociation in water is

$$1b_2^1 3a_1^1 4a_1^1 2b_2^1, \tag{24}$$

which becomes low in energy as the bonds are stretched. The $1b_2$ and $2b_2$ have σ_{OH} and σ^*_{OH} character. The $3a_1$ and $4a_1$ orbitals also have such character, though also mixed with oxygen lone pair character near the equilibrium geometry. Near equilibrium, the leading configuration of the ground electronic state is $1b_2^2 3a_1^2$. As the O–H distance increases, the gap between the $4a_1/2b_2$ and $1b_2/3a_1$ orbitals decreases, and configurations involving all four orbitals become important. The 2SF ansatz, which includes all leading electronic configurations and exploits a well-behaved high-spin quintet reference, is capable of describing these changes in the ground-

TABLE I. Total FCI energies (hartrees) and energy differences (mhartrees) with respect to FCI for the symmetric bond breaking of the water molecule. The last line summarizes NPEs. The molecular angle is fixed at 109.57° and R_e=0.9929 Å.

r_{OH} (R_e)	FCI[a]	CASSCF(6e, 5o)[a]	CCSDT[a]	2SF-CC(2,3)	2SF-CC(2,$\tilde{3}$)	2SF-CCSD	2SF-CIDT	2SF-CID$\tilde{T}$	2SF-CID	2SF-CIS
1.0	−76.238 85	162.99	0.51	2.04	3.64	143.62	68.23	69.90	222.94	227.99
1.4	−76.099 02	153.45	1.23	0.00	2.25	90.06	65.61	68.05	165.56	170.15
1.8	−75.978 14	138.12	1.34	−0.61	1.52	51.51	60.54	63.50	136.37	141.11
2.2	−75.927 22	127.76	−11.48	−0.64	1.32	17.60	48.16	52.28	119.95	124.56
2.6	−75.913 41	124.04	−30.56	−0.59	0.74	4.24	40.88	45.53	111.87	116.34
3.0	−75.910 03	123.01	−41.06	−0.60	−0.10	0.62	38.65	43.48	109.09	113.60
3.4	−75.909 08	122.71	−46.25	−0.53	−0.53	−0.36	38.04	42.90	108.27	112.73
3.8	−75.908 78	122.61	−48.91	−0.67	−0.67	−0.62	37.87	42.72	108.04	112.44
NPE (kcal/mol)		25.3	31.5	1.7	2.7	90.5	19.1	17.1	72.1	72.5

[a]From Ref. 63.

state wave function in the entire range of nuclear displacements.

Table I gives energy differences of the ground electronic state of water relative to the FCI total energy. It also presents the corresponding maximum nonparallelity errors (NPEs), which characterize the quality of the entire curve. The potential energy profiles are visualized in Fig. 1.

The behavior of the CCSDT curve is very similar to that of CCSD(T) in well-studied cases of single bond-breaking.[64] It follows the FCI curve very closely until large O–H distances, where it exhibits an unphysical turn over, which is responsible for its large NPE of 32 kcal/mol. The shape of the CASSCF curve is qualitatively correct, but due to lack of dynamical correlation, the resulting NPE is quite large (25 kcal/mol) and the error decreases towards dissociation.

The full space and active space 2SF-CC(2,3) curves are very close to each other (as well as to FCI), with respective NPEs of 1.7 and 2.7 kcal/mol. Interestingly, the absolute errors of 2SF-CIDT are much larger than those of 2SF-CC(2,3), which suggests that the similarity transformation results in higher accuracy even though it is not required for size intensivity. The NPEs of the 2SF-CIDT models are 17 and 19 kcal/mol, respectively. Thus, correlation effects included through similarity transformations in the EOM counterpart of these methods reduce the NPEs by about a factor of 10 in these triples methods. A comparison between 2SF-CID and 2SF-CCSD also shows a large reduction in absolute errors due to the similarity transformation—between 75 and 100 kcal/mol.

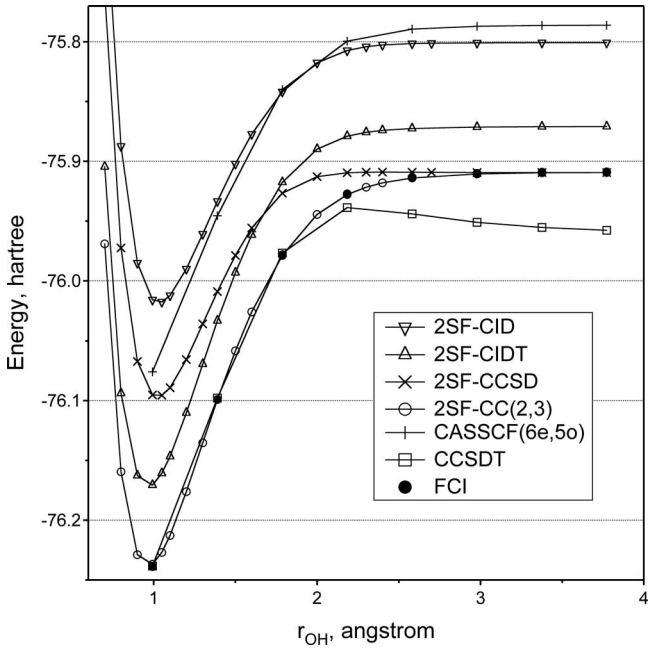

FIG. 1. Potential energy curves along symmetric stretch coordinate of water (r_{OH}). For a better comparison between methods, absolute energies (hartree) have been plotted. The curves of the active space 2SF models are indistinguishable from their full space counterparts on this scale.

At the dissociation limit, where the wave function acquires tetraradicaloid character, the differences between 2SF-CCSD, 2SF-CC(2,3), and FCI total energies are less than 1 mhartree. However, the absence of triple excitations in 2SF-CCSD becomes noticeable at shorter distances, and its accuracy deteriorates. This is partly due to increased importance of dynamical correlation around equilibrium,[7] but since the effect is twice as large as the dynamical correlation error measured by CASSCF, we must conclude that it also involves nondynamical correlation. Evidently triple substitutions in 2SF are crucial for recovering nondynamical correlation when the quintet reference is much higher in energy. A similar trend is observed for the 2SF-CI models, although in this case there is a fairly large gap (about 65 kcal/mol) between 2SF-CID and 2SF-CIDT at the dissociation limit. The large NPEs values for the models without triple excitations reflect the importance of $\hat{R}_3$ for the balanced description of the entire curve.

The difference between 2SF-CID and 2SF-CIS is very small, both in terms of absolute energies and NPEs. It suggests that 2SF-CIS can be used as a well-behaved zero order wave function for including the effects of higher excitations perturbatively.

The accuracy of the 2SF methods depends on the quality of the quintet reference, which can be monitored by calculation of $\langle \hat{S}^2 \rangle$. In this example, the spin contamination of the UHF and, consequently, CCSD wave functions is small for the entire range of distortions. The corresponding $\langle \hat{S}^2 \rangle$ values are 6.004–6.006 and 6.002–6.003, respectively.

The spin contamination of the 2SF-CIS singlet ground state increases with the O–H distance and the wave function at dissociation has $\langle \hat{S}^2 \rangle$ that corresponds to a triplet state. Although this sounds alarming, there is no energetic conse-

TABLE II. Excitation energies (in kcal/mol) with respect to the singlet ground state $1\ ^1\Sigma_g^+$ of linear H_4 at three different H–H distances. The difference between the full and active space 2SF models is shown in parentheses.

State	EOM-CC(2, 3)	2SF-CC(2, 3)	2SF-CCSD	2SF-CIDT	2SF-CID
			d=1.0 Å		
$2\ ^1\Sigma_g^+$	221.7	221.7(0.0)	230.9	222.0(0.0)	231.0(−0.2)
$1\ ^3\Sigma_u^+$	113.5	113.3(0.0)	108.7	113.4(0.0)	108.7(0.2)
$1\ ^3\Sigma_g^+$	221.9	222.9(0.0)	213.9	222.0(0.0)	214.2(0.4)
$2\ ^3\Sigma_u^+$	333.6	333.7(0.0)	333.4	333.7(0.0)	334.1(0.7)
$1\ ^5\Sigma_g^+$	444.2	443.9(0.0)	422.2	444.5(0.0)	422.8(1.2)
			d=2.0 Å		
$2\ ^1\Sigma_g^+$	37.9	29.9(0.0)	28.3	30.0(0.0)	28.4(0.3)
$1\ ^3\Sigma_u^+$	14.7	11.7(0.0)	11.1	11.7(0.0)	11.1(0.1)
$1\ ^3\Sigma_g^+$	27.1	24.2(0.0)	22.9	24.2(0.0)	22.9(0.1)
$2\ ^3\Sigma_u^+$	40.0	37.2(0.0)	35.1	37.2(0.0)	35.2(0.2)
$1\ ^5\Sigma_g^+$	46.3	43.4(0.0)	40.9	43.4(0.0)	41.0(0.3)
			d=3.4 Å		
$2\ ^1\Sigma_g^+$	1.3	0.4(0.0)	0.4	0.4(−0.2)	0.4(0.0)
$1\ ^3\Sigma_u^+$	1.0	0.2(0.0)	0.2	0.2(0.0)	0.2(0.0)
$1\ ^3\Sigma_g^+$	1.1	0.5(0.0)	0.3	0.5(−0.1)	0.3(0.0)
$2\ ^3\Sigma_u^+$	1.4	0.5(0.0)	0.5	0.5(−0.1)	0.5(0.0)
$1\ ^5\Sigma_g^+$	11.0	0.6(0.0)	0.6	0.6(0.0)	0.6(0.0)

quences because the singlet, triplet, and quintet are degenerate at dissociation. Due to the degeneracy, small deviations from spin purity in the high-spin reference result in large spin contamination in the M_s=0 manifold. SF-CIS exhibits similar behavior in single bond-breaking.

C. H_4

The hypothetical stretched H_4 molecule is arguably the simplest example of a molecular tetraradical. Among tetrahedral, square planar or linear structures, linear $D_{\infty h}$ is the least energetically unfavorable arrangement (with respect to two hydrogen molecules).[65] Thus, we consider homogeneously distributed, linear H_4, and compute the energies of the several low-lying states as function of the interatomic distance d. The reference configuration used in all 2SF calculations is

$$1\sigma_g^1 1\sigma_u^1 2\sigma_g^1 2\sigma_u^1, \tag{25}$$

and 2SF excitations generate target wave functions for the fully symmetric singlet ground state ($1\ ^1\Sigma_g^+$), as well as singlet, triplet, and quintet excited states as shown in Table II. The spin coupling between the four paramagnetic centers decreases with d, and becomes negligible beyond 2.5 Å, where the two singlet, three triplet, and the quintet eigenstates corresponding to four unpaired electrons become essentially degenerate.

Potential energy curves for the ground state are visualized in Fig. 2, which also shows the results for unrestricted HF, Möller–Plesset perturbation theory (MP2), and CCSD. The behavior of the UHF, UMP2, and UCCSD curves is very similar to well-studied cases of single bond-breaking.[64] The UCCSD curve is qualitatively correct, but the corresponding dissociation energy (D_e) is underestimated. The UMP2 curve exhibits an unphysical shape in the intermediate region.

All 2SF curves are smooth and exhibit qualitatively correct behavior. The models with triple excitations agree very well with each other, e.g., for the $1\ ^1\Sigma_g^+$ ground state, the difference between 2SF-CIDT and 2SF-CC(2,3) does not exceed 1 kcal/mol. Thus, the similarity transformation does not make a big difference for this four-electron system. Figure 2 shows only the 2SF-CC curves, because 2SF-CI results are indistinguishable on this scale. 2SF-CID and 2SF-CCSD

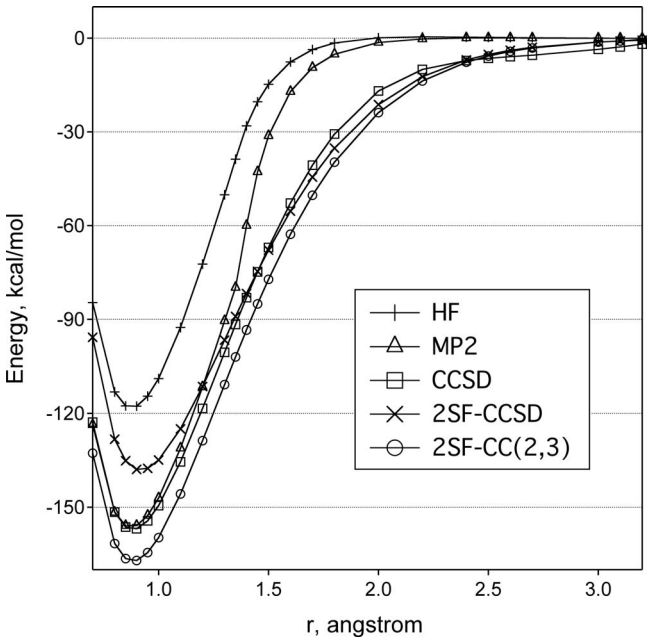

FIG. 2. Potential energy curves for the ground electronic state ($1\ ^1\Sigma_g^+$) along symmetric stretch coordinate of linear H_4. All curves are shifted such that they approach zero at large distances. The 2SF-CID and 2SF-CIDT curves are indistinguishable from their 2SF-CC counterparts, therefore, they were not included.

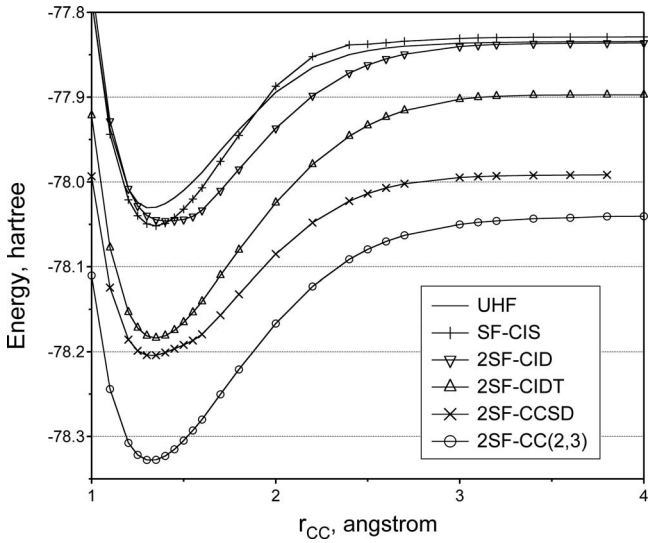

FIG. 3. Potential energy curves along the C=C bond breaking coordinate of ethylene. For a better comparison between methods, absolute energies (hartree) have been plotted.

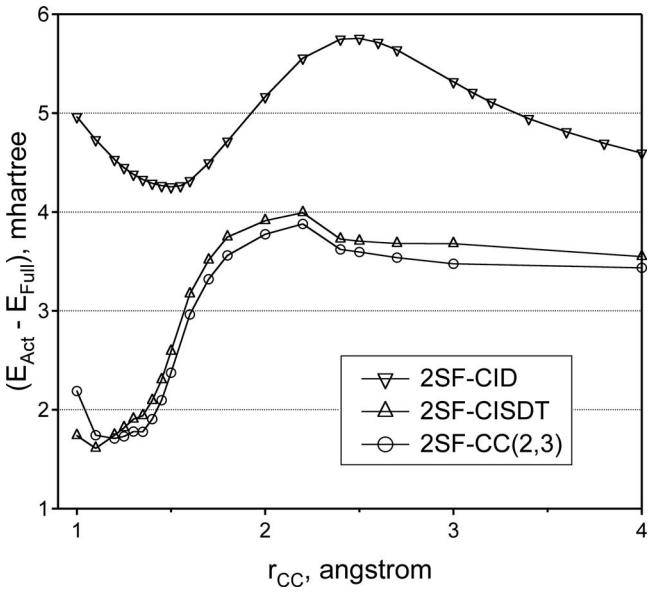

FIG. 4. Energy difference between full and active 2SF methods ($E_{act}-E_{full}$) along the C=C bond breaking coordinate of ethylene.

underestimate D_e by about 30 kcal/mol suggesting that higher excitations are important for quantitative description even in a four-electron system.

Despite the small number of electrons, the differences between the 2SF and non-spin-flip EOM-CC(2,3) transition energies are perceivable—they are very small at short distances, but gradually increase to up to 10 kcal/mol as the single reference description of the singlet ground state deteriorates.

2SF-CCSD and 2SF-CID excitation energies show larger differences of up to 20 kcal/mol (Table II). As in the previous example, differences are larger at short distances due to the importance of nondynamical correlation.[7] On the other hand, at large d, even 2SF-CIS values are within tenths of kcal/mol of 2SF-CC(2,3).

All active space approximations of 2SF models are very close to their full space counterparts for all distances. For 2SF-CC(2,3), the difference is less than tenths of a kcal/mol, whereas for 2SF-CIDT 0.1–0.2 kcal/mol differences are observed at large d. The largest difference between 2SF-CID and its active space approximation, 2SF-CIS, is 1.2 kcal/mol.

D. Double bond-breaking: Ethylene dissociation

This section presents the 2SF calculations of the double bond-breaking in ethylene. We also use this example to compare the performance of 2SF against UHF and SF-CIS models. Potential energy scans along the C=C bond-breaking coordinate are summarized in Fig. 3. The 2SF calculations employed the $3a_g^1 1b_{3u}^1 1b_{2g}^1 3b_{1u}^1$ UHF quintet reference, with $\langle S^2\rangle$ values of 6.005–6.017. All 2SF curves are smooth and the relative energetics between models are very similar to the water case. While the 2SF methods with triple excitations, 2SF-CIDT, and 2SF-CC(2,3), appear quite parallel to each other, the absence of $\hat{R}_3$ in 2SF-CCSD and 2SF-CID has important effects at small r_{CC}. As in the previous examples, the results of the active space 2SF methods are remarkably close to their full space counterparts, i.e., the absolute energy differences are less than 4 mhartree for the 2SF-CIDT and 2SF-CC(2,3) methods, and less than 6 mhartree for 2SF-CID (Fig. 4).

The dissociation profiles of UHF, SF-CIS, and 2SF-CID (and 2SF-CIS) are within the same energy range. At $1.3 < r_{CC} < 1.6$ Å, SF-CIS is lower than UHF due to its ability to capture the diradicaloid character of the wave function. In this region, 2SF-CID suffers from the lack of triple excitations. These three methods are very close to each other, the main discrepancies being observed at intermediate distances ($1.6 < r_{CC} < 2.7$ Å), where both UHF and SF-CIS energies increase too fast with r_{CC}. The energies at dissociation limit are very similar for the three curves.

Although energies of the UHF, SF-CIS, and 2SF-CID dissociation curves are very similar, both at intermediate and especially at long C–C distances, their wave functions are considerably different. The 2SF-CID wave function, which is derived from the well defined $M_s=2$ quintet via 2SF excitations, includes all leading configurations of the total singlet wave function. Contrary to that, the single-determinantal wave function of the high-spin triplet employed as the reference in SF and the UHF singlet are incomplete. The analysis of atomic spin charges along the dissociation coordinates provides a clue on the nature of this incompleteness. Figure 5 presents the difference between the spin charges of the methylene fragments ($\Delta\rho_s$) computed from the Mulliken atomic spin charge contributions.

The spatial symmetry of the UHF singlet wave function breaks at C–C distances larger than 1.30 Å. The spin charge difference between the two fragments increases up to 4 a.u. which corresponds to the superposition of the two triplets ($M_s=\pm 2$). At dissociation, this spin incomplete wave function can be described as a mixture of the degenerate $M_s=0$ singlets, triplets, and quintet states.

The spatial symmetry of the reference triplet is only preserved for $r_{CC} < 2.0$ Å. The $\Delta\rho_s=2$ a.u. value at dissociation

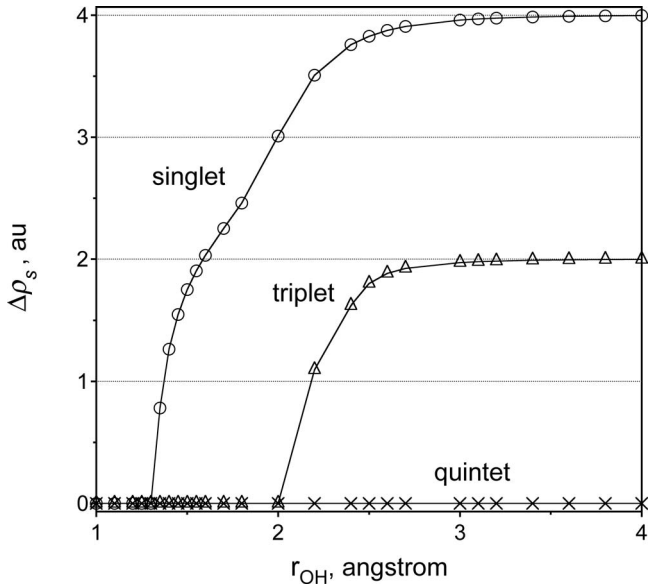

FIG. 5. Mulliken spin charge difference ($\Delta\rho_s$) between the two methylene fragments for the singlet (circles), triplet (triangles), and quintet (crosses) UHF wave functions (M_s=0, 1, and 2, respectively) along the C=C bond breaking coordinate of ethylene.

corresponds to the superposition of a high-spin triplet and a highly spin contaminated singlet. These problems in the triplet reference are inherited by the final SF-CIS wave function, which resembles the UHF solution in the sense of its spin incompleteness.

E. Trimethylenemethyl diradical

In the TMM diradical,[66–72] four π-electrons are distributed in four molecular π-type orbitals as shown in Fig. 6. Most of the low-lying TMM states can be accurately described[32,41,72] by single SF methods using the triplet reference shown in Fig. 6. Alternatively, these states can be described by 2SF using the quintet $1b_1^1 2b_1^1 1a_2^1 3b_1^1$ reference. In active-space calculations, the active space included all singly occupied orbitals, i.e., $1b_1^1 2b_1^1 1a_2^1 3b_1^1$.

A high level of correlation is important for this system. Indeed, the inclusion of triples in EOM-SF-CC (SF-CC) changes the energies of all three excited states by 0.15–0.3 eV (Table III). SF-CCSD overestimates the energies of the two closed shell singlets, whereas the open shell (and highly spin contaminated) $^1B_1$ is over stabilized. The 2SF-CC(2,3) excitation energies are in between the SF-CCSD and SF-CC(2,3) values suggesting that 2SF-CC(2,3) recovers less correlation than SF-CC(2,3). This can be easily rationalized considering that in 2SF double excitations generate leading configurations of the target wave function, and triples describe dynamical correlation, whereas in SF the target state is reached through single spin-flipping excitations and doubles and triples correlate it. Thus, single SF methods employing the triplet $1b_1^2 2b_1^1 1a_2^1 3b_1^0$ reference are a better methodological choice for TMM: Double spin-flip methods are most effective for the cases where the high spin triplet reference of single spin-flip methods is not well described as a single configuration.

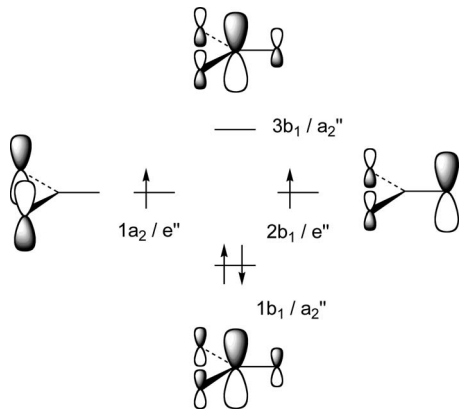

FIG. 6. Frontier MOs of TMM.

It is encouraging that the active space 2SF results closely follow the full 2SF values, which can be exploited to extend 2SF to larger species and/or basis sets. In TMM, the basis set convergence is state dependent. Whereas in the two lowest states, namely, $^1B_1$ and $1\,^1A_1$, the increase of the basis set from 6-31G* to cc-pVTZ affects the excitation energies by only 0.01–0.03 eV; there is a 0.5 eV drop in the excitation energy of the $2\,^1A_1$ state computed with SF-CC and 2SF-CC. This effect is considerably lower in 2SF-CIS and 2SF-CID (0.05 and 0.10 eV, respectively).

F. 2,5-didehydrometaxylylene tetraradical

DDMX is a model aromatic tetraradical, related to the *meta*-xylylene (MX) and *para*-benzyne diradicals. The DDMX's frontier MOs consist of a pair of π orbitals, similar to those of MX, and two σ a_1 orbitals as in *p*-benzyne (see

TABLE III. Total energies of the ground state (hartree) and adiabatic excitation energies (eV) of the TMM diradical calculated by SF, 2SF, and multireference methods.

Method	$^3B_2$	$^1B_1$	$1\,^1A_1$	$2\,^1A_1$
	6-31G* basis			
SF-CCSD	−155.365 751	0.510	0.919	4.337
SF-CC(2,$\bar{3}$)[b,c]	−155.370 897	0.657	0.784	4.171
SF-CC(2,3)[c]	−155.373 271	0.653	0.774	4.028
2SF-CIS	−154.897 669	0.737	0.906	4.659
2SF-CID	−154.899 296	0.617	0.901	4.636
2SF-CC(2,$\bar{3}$)[b]	−155.402 117	0.610	0.856	4.338
2SF-CC(2,3)	−155.402 704	0.608	0.856	4.333
	cc-pVTZ basis			
SF-CCSD	−155.589 945	0.554	0.933	3.860
SF-CC(2,3)[extrapolated]	−155.597 465	0.697	0.788	3.551
2SF-CIS	−154.950 187	0.695	0.895	4.613
2SF-CID	−154.954 683	0.624	0.885	4.528
2SF-CC(2,$\bar{3}$)[b]	−155.598 750	0.628	0.831	3.889
CASSCF(10/10)[a]	−155.033 829	0.705	0.832	
MCQDPT(10/10)[a]	−155.568 282	0.710	0.828	
Experiment[e] −ΔZPE[a]			0.787	

[a]Equilibrium geometries and ZPEs of TMM's states as long as multireference data are from Ref. 72; four frozen core and four frozen virtual orbitals.
[b]Four orbital active space; see text for detail.
[c]From Ref. 32.
[d]Extrapolated results From Ref. 32.
[e]Reference 68.

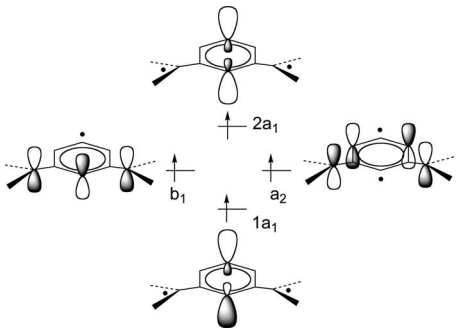

FIG. 7. Frontier MOs of DDMX.

Fig. 7). The distribution of four electrons into these four orbitals defines the electronic states of DDMX. According to the spin polarization rule (and by analogy to MX and *para*-benzyne), the ground state of DDMX should be the triplet $^3B_2$, with two σ-electrons coupled antiferromagnetically and two π-electrons coupled ferromagnetically. Note that this $^3B_2$ triplet state has multiconfigurational wave function since the pair of σ-electrons can occupy either of a_1 orbitals. Thus, the only well-behaved single reference state is the $^5B_2$ quintet, where each electron occupies its own tetraradical orbital, i.e., $1a_1^1b_1^1a_2^12a_1^1$. We use this state as the reference in 2SF calculations.

The vertical excitation energies of DDMX are summarized in Table IV. In agreement with the spin polarization principle, the lowest electronic state by most of the methods is indeed the $1\,^3B_2$ triplet, with the $^5B_2$ quintet about 0.2–0.3 eV higher in energy for the highly accurate ROHF-based 2SF-CC$(2,\tilde{3})$, CASSCF(10/10), and MCQDPT(10/10) methods. This energy difference is similar to the 0.165 ± 0.016 singlet-triplet energy splitting in *p*-benzyne.[41] The open shell singlet of the same symmetry with four unpaired electrons ($1\,^1B_2$) is 0.3–0.7 eV higher in energy, whereas the singlet with the doubly occupied a_1 orbital and the singly occupied b_1 and a_2 orbitals ($2\,^1B_2$) is 1.2–1.8 eV higher. The latter energy splitting is in agreement with the 1.2 eV excitation energy of the $^1B_2$ open shell singlet in MX.[73] The lowest states of A_1 symmetry are also related to the MX and *p*-benzene electronic states. For example, the closed shell $^1A_1$ singlet, in which two electrons doubly occupy either of the a_1 orbitals and two other electrons are in either b_1 or a_2 orbitals, resembles a combination of closed shell singlet of *p*-benzyne plus the closed shell singlet of MX. In the $^3A_1$ triplet, the π electrons produce a closed shell singlet, while the σ electrons have triplet coupling, as in the triplet state of *p*-benzyne.

Excited states of the A_2 and B_1 symmetries are unique to DDMX because here the electronic density is transferred between σ and π shells. Very low in energy is a pair of the A_2 singlet and triplet states. In these states, two electrons occupy the lowest $1a_1$ orbital, and two other electrons reside on $2a_1$ and a_2. In the B_1 singlet and triplet, $2a_1$ and b_1 are singly occupied. Electronic densities of the $1a_1$ and b_1 MOs overlap, which results in energetically favorable $b_1\rightarrow 1a_1$ transition and low excitation energies of the A_2 states. In contrast, the $a_2\rightarrow 1a_1$ transition involves charge transfer. That is why the B_1 states are significantly higher in energy. Another interesting observation related to the shape and interaction of MOs is the relative order of the singlet and triplet states of A_2 and B_1 symmetries. In the A_2 pair, the singlet is slightly lower than the triplet, whereas the order is reversed in the B_1 manifold. In the B_1 states, electronic densities of the singly occupied $2a_1$ and b_1 orbitals overlap and Hund's rule favors the high spin triplet configuration. However, densities of $2a_1$ and a_2, singly occupied in the A_2 states, do not overlap and Hund's rule is not applicable here. Instead, the order of the states is governed by the correlation effects that usually stabilize the singlet coupling, as indeed occurs in the A_2 singlet-triplet pair.

As in related didehydrotoluenes and dehydro-*meta*-xylylene,[74] the electronic states of DDMX suffer from strong spin contamination when using UHF reference ($S^2=6.56$). The spin contamination originates from the instabilities in the σ-π type high spin state used as the 2SF reference. To reduce the spin contamination of the target states, we employ the ROHF quintet reference. This results in the changes in energy differences up to 0.5 eV. Since the 2SF-CID and 2SF-CIDT results are obtained with the UHF

TABLE IV. Total energies of the ground state (hartree) and vertical excitation energies (eV) of the DDMX tetraradical calculated by 2SF and multireference methods. At the B3LYP/cc-p VTZ equilibrium geometry of the $^5B_2$ quintet, all excited state calculations are performed in the 6-31G* basis.

Method	$1\,^3B_2$	$^1A_1$	$^1A_2$	$^1B_1$	$1\,^1B_2$	$2\,^1B_2$	$^3A_1$	$^3A_2$	$^3B_1$	$2\,^3B_2$	$^5B_2$
2SF-CID	−306.250 773	1.318	0.800	4.661	0.742	1.848	2.198	2.586	3.159	1.219	
2SF-CIDT[a]	−306.366 012	0.888	0.088	1.929	0.312		1.711	0.862	1.345		0.874
2SF-CC$(2,\tilde{3})$[a]	−307.190 059	1.255	0.392	2.283	0.531	1.768	1.728	1.186	2.179	1.431	0.629
2SF-CC$(2,\tilde{3})$[a,b]	−307.203 133	1.299	0.413	2.161	0.625	1.707	1.549	0.729	1.982	0.938	0.309
CASSCF(4/4)[c]	−306.192 600	1.581	0.422	3.188	0.514	1.757	1.621	0.334	2.741	0.394	−0.119
MRCI(4/4)[c]	−306.980 518	1.134	0.126	2.198	0.438	1.516	1.237	0.125	2.205	0.431	−0.148
CASSCF(10/10)[d]	−306.312 918	1.547	0.730	2.550	0.642	1.623	0.833	0.833	2.290	0.693	0.192
MCQDPT(10/10)[d]	−307.199 675	0.382	0.133	1.178	0.480	1.264	0.829	0.300	1.159	0.575	0.219

[a]Four orbital active space, see text for detail.
[b]ROHF quintet as reference.
[c]Active space consists of two π and two radical σ orbitals and four active electrons; two electronic states of each multiplicity and each symmetry were found and root-averaged.
[d]Active space consists of eight π and two radical σ orbitals and ten active electrons; two electronic states of each multiplicity and each symmetry were found and root-averaged.

reference, they are less accurate. We were not able to employ the quintet ROHF reference for 2SF-CI calculations because of severe convergence problems in the Davidson diagonalization procedure.

Comparing the 2SF results with multireference data is not straightforward. The CASSCF and MRPT values in the 10/10 active space differ by as much as 1.4 eV, which suggests that neither of these techniques is reliable in this case with the active space chosen. The small 4/4 active space used in the MRCI calculations is not suitable for the description of relative ordering of multiplets of the same symmetry, such as $^5B_2-{}^3B_2$ and $^3A_2-{}^1A_2$. CASSCF (and, consequently, MRCI) in minimal active spaces is known to overstabilize states of higher multiplicities, i.e., quintet versus triplet or triplet versus singlet (see, for example, discussion in Ref. 70), as indeed happens in DDMX. Differences between ROHF-based 2SF-CC$(2,\tilde{3})$ and MRPT range from 0.1 to 1.0 eV and the biggest deviations are observed for the states where the disagreement between CASSCF and MRPT values is the largest. There is a somewhat better agreement between 2SF-CC$(2,\tilde{3})$ and MRCI, with exception of the state ordering in $^5B_2-{}^3B_2$ and $^3A_2-{}^1A_2$ pairs.

IV. CONCLUSIONS

We have extended the spin-flip (SF) approach to double bond-breaking and tetraradicals. The corresponding target multiconfigurational wave functions, which are of the four electrons in four orbitals type, are described as double spin-flipping excitations from a high spin quintet reference. We considered EOM-2SF-CC (or 2SF-CC) and 2SF-CI methods including up to triple excitations, as well as active space approximations. 2SF is a multistate approach capable of describing several electronic states (any states whose primary electron configurations are contained within the active space), which is particularly important for tetraradical and tetraradicaloid systems with several low-lying electronic states.

The results of active space variants of all 2SF models are in excellent agreement with their full space counterparts, which is very encouraging in view of the greatly reduced scaling of the active space models. For example, our simplest and least expensive 2SF model (2SF-CIS) has a quadratic number of amplitudes rather than the quartic number without the active space approximation. 2SF-CIS will therefore be potentially applicable to large molecules, just like the conventional CIS method.

We have found that inclusion of triple excitations is important for achieving quantitative results with the 2SF models, especially around equilibrium geometries. One relatively feasible strategy would be to employ active space 2SF methods with the reduced subset of triples, which will result in a model that scales as N^6. Alternatively, a perturbative treatment of the triple excitations might be explored.

ACKNOWLEDGMENTS

This work benefited from the resources of the iOpenShell Center for Computational Studies of Electronic Structure and Spectroscopy of Open-Shell and Electronically Excited Species (iopenshell.usc.edu) supported by the National Science Foundation through the CRIF:CRF CHE-0625419 +0624602+0625237 grant. One of the authors (A.I.K.) also gratefully acknowledges support of the National Science Foundation through the CHE-0616271 grant. Two of the authors (M.H.G. and D.C.) are supported by the Office of Basic Energy Sciences of the U.S. Department of Energy through the LBL Ultrafast Center, with additional support from the Director, Office of Energy Research, Office of Basic Energy Sciences, Chemical Sciences Division of the U.S. Department of Energy under Contract No. DE-AC0376SF00098, and supercomputer time from NERSC. One of the authors (D.C.) acknowledges financial support from a Fulbright Fellowship.

APPENDIX: SIZE INTENSIVITY IN SPIN-FLIP METHODS

This appendix discusses size consistency, i.e., additive separability of the energy in the limit of noninteracting fragments,[14] of the spin-flip methods. Specifically, we are interested in the scaling properties of spin-flip excitation energies of a subsystem $\boldsymbol{A}$ in the presence of a subsystem $\boldsymbol{B}$ in its ground state at infinite distance. This is a property that must remain independent of the size of the system, therefore it is rigorously referred as *size intensivity*.[22] The proof and discussion presented here generalizes the ideas and results from Refs. 14, 22, and 36 to the EOM-*n*SF-CC and *n*SF-CI cases.

In the following analysis we employ the EOM-*n*SF-CC and CC generic expressions in Eqs. (A1)–(A3), respectively. The same equations describe *n*SF-CI as the case when the cluster operator vanishes, i.e., $\hat{T}=0$.

$$\langle 0|\hat{x}e^{-\hat{T}}(\hat{H}-E)e^{\hat{T}}\hat{R}|0\rangle = 0, \tag{A1}$$

$$\langle 0|e^{-\hat{T}}(\hat{H}-E^{(0)})e^{\hat{T}}|0\rangle = 0, \tag{A2}$$

$$\langle 0|\hat{x}e^{-\hat{T}}\hat{H}e^{\hat{T}}|0\rangle = 0. \tag{A3}$$

In Eqs. (A1)–(A3) E and $E^{(0)}$ are the EOM and CC energies, $|0\rangle=\hat{0}|\text{vac}\rangle$ is the Hartree–Fock reference, $\hat{R}$ the SF excitation operator, and $\hat{x}^\dagger$ is an excitation operator with respect to the reference determinant.

SF excitation energy of system $\boldsymbol{A}$ is not affected by system $\boldsymbol{B}$ at infinite distance, $E_{AB}=E_A+E_B^{(0)}$, only if the composite system obeys the following:

$$\begin{aligned} 0 = {} & \langle 0_A|\hat{x}_A e^{-\hat{T}_A}(\hat{H}_A - E_A)e^{\hat{T}_A}\hat{R}_A|0_A\rangle\langle 0_B|\hat{x}_B e^{-\hat{T}_B}e^{\hat{T}_B}\hat{R}_B|0_B\rangle \\ & + \langle 0_A|\hat{x}_A e^{-\hat{T}_A}e^{\hat{T}_A}\hat{R}_A|0_A\rangle\langle 0_B|\hat{x}_B e^{-\hat{T}_B}(\hat{H}_B \\ & - E_B^{(0)})e^{\hat{T}_B}\hat{R}_B|0_B\rangle, \end{aligned} \tag{A4}$$

where operator relations at the limit: $\hat{H}_{AB}=\hat{H}_A+\hat{H}_B$, $\hat{T}_{AB}=\hat{T}_A+\hat{T}_B$, $\hat{R}_{AB}=\hat{R}_A+\hat{R}_B$, and $\hat{x}_{AB}=\hat{x}_A\hat{x}_B$, and their commutator properties[75] have been applied to Eq. (A1).

Only SF excitations localized on subsystem $\boldsymbol{A}$ needed to be considered. Other SF excitations correspond to either

charge transfer or SF excitations on $\boldsymbol{B}$, which do not couple with the SF excited states of $\boldsymbol{A}$. The validity of Eq. (A4) is investigated below considering the different possibilities for the $\hat{x}_A$ and $\hat{x}_B$ de-excitation operators.

Case $\hat{x}_A=1$. The right hand-side of Eq. (A4) vanishes due to different left/right spin multiplicities of the $\boldsymbol{A}$ terms.

Case $\hat{x}_A \neq 1$ and $\hat{x}_B=1$. If $\hat{R}_B=1$, the first and the second terms of Eq. (A4) reduce to EOM-nSF-CC (nSF-CI) of $\boldsymbol{A}$ and CC (HF) of $\boldsymbol{B}$ equations. If $\hat{R}_B \neq 1$, the first term is zero due to orthogonality between $|0_B\rangle$ and $\hat{R}_B|0_B\rangle$. The second term reduces to Eq. (A5) and requires a further analysis.

$$\langle 0_B|e^{-\hat{T}_B}(\hat{H}_B - E_B^{(0)})e^{\hat{T}_B}\hat{R}_B|0_B\rangle = 0. \tag{A5}$$

For general EOM-nSF-CC, this term does not vanish and Eq. (A5) is not satisfied. For nSF-CI, it is valid if $\hat{R}_B$ contains up to single excitations and the ground state of $\boldsymbol{B}$ obeys Brillouin's theorem.

Case $\hat{x}_A \neq 1$ and $\hat{x}_B \neq 1$. If $\hat{R}_B=1$, the first term of Eq. (A4) corresponds to EOM-nSF-CC (nSF-CI) of fragment $\boldsymbol{A}$. The second term reduces to Eq. (A6), and when $\hat{T}_B \neq 0$ it vanishes by virtue of the CC ground state equation of system $\boldsymbol{B}$. For nSF-CI, it is zero only if $\hat{x}_B$ is restricted to single de-excitations and Brillouin's theorem for $\boldsymbol{B}$ holds true,

$$\langle 0_B|\hat{x}_B e^{-\hat{T}_B}(\hat{H}_B - E_B^{(0)})e^{\hat{T}_B}|0_B\rangle = 0. \tag{A6}$$

The case with $\hat{R}_B \neq 1$ corresponds to excitations on both fragments. In EOM-nSF-CC, due to the fact that the $\hat{R}_B=1$ ($x_A \neq 1$ and $x_B \neq 1$) cases are all zero, the eigenvectors with $\hat{R}_B \neq 1$ do not couple with the eigenvectors of the $\boldsymbol{A}$ spectrum,[22] even considering that Eq. (A5) does not apply. In other words, these correspond to new roots involving simultaneous excitations on $\boldsymbol{A}$ and $\boldsymbol{B}$, but the localized excitations on $\boldsymbol{A}$ are not affected. In the nSF-CI case, the same conclusion can be reached under the above mentioned conditions on Eq. (A6).

In conclusion, we have proven that size intensivity is preserved in EOM-nSF-CC. The key requirement is the validity of CC equation on fragment $\boldsymbol{B}$ [Eq. (A6)], which is sufficient although Eq. (A5) is nonzero. On the other hand, size intensivity in nSF-CI requires two conditions: the presence of no more than single non-SF excitations in the wave function and the noninteraction between the reference determinant and singly excited configurations (Brillouin's theorem) of the ground state fragments. These two conditions are necessary in Eqs. (A5) and (A6).

The above results do not depend on the number of spin-flip excitations present at a time in the excitation operator, and they are general for any single reference nSF method.

[1] B. O. Roos, P. R. Taylor, and P. E. M. Siegbahn, Chem. Phys. **48**, 157 (1980).
[2] K. Ruedenberg, M. W. Schmidt, M. M. Gilbert, and S. T. Elbert, Chem. Phys. **71**, 41 (1982).
[3] *Recent Advances in Multi-reference Methods*, edited by K. Hirao (World Scientific, Singapore, 1999).
[4] D. Mukherjee and S. Pal, Adv. Quantum Chem. **20**, 291 (1989).
[5] R. J. Bartlett, Int. J. Mol. Sci. **3**, 579 (2002).
[6] F. A. Evangelista, W. D. Allen, and H. F. Schaefer, J. Chem. Phys. **125**, 154113 (2006); provides an overview of different MR-CC approaches and gives numerical examples.
[7] A. I. Krylov, C. D. Sherrill, E. F. C. Byrd, and M. Head-Gordon, J. Chem. Phys. **109**, 10669 (1998).
[8] S. R. Gwaltney, C. D. Sherrill, M. Head-Gordon, and A. I. Krylov, J. Chem. Phys. **113**, 3548 (2000).
[9] K. Kowalski and P. Piecuch, J. Chem. Phys. **113**, 8490 (2000).
[10] A. I. Krylov, Annu. Rev. Phys. Chem. **59**, 433 (2008).
[11] D. J. Rowe, Rev. Mod. Phys. **40**, 153 (1968).
[12] K. Emrich, Nucl. Phys. A **351**, 379 (1981).
[13] J. Geertsen, M. Rittby, and R. J. Bartlett, Chem. Phys. Lett. **164**, 57 (1989).
[14] J. F. Stanton and R. J. Bartlett, J. Chem. Phys. **98**, 7029 (1993).
[15] S. V. Levchenko and A. I. Krylov, J. Chem. Phys. **120**, 175 (2004).
[16] D. Sinha, D. Mukhopadhyay, and D. Mukherjee, Chem. Phys. Lett. **129**, 369 (1986).
[17] S. Pal, M. Rittby, R. J. Bartlett, D. Sinha, and D. Mukherjee, Chem. Phys. Lett. **137**, 273 (1987).
[18] J. F. Stanton and J. Gauss, J. Chem. Phys. **101**, 8938 (1994).
[19] M. Nooijen and R. J. Bartlett, J. Chem. Phys. **102**, 3629 (1995).
[20] H. J. Monkhorst, Int. J. Quantum Chem., Symp. **11**, 421 (1977).
[21] H. Sekino and R. J. Bartlett, Int. J. Quantum Chem., Symp. **18**, 255 (1984).
[22] H. Koch, H. J. Aa. Jensen, P. Jørgensen, and T. Helgaker, J. Chem. Phys. **93**, 3345 (1990).
[23] M. Head-Gordon and T. J. Lee, in *Modern Ideas in Coupled Cluster Theory*, edited by R. J. Bartlett (World Scientific, Singapore, 1997).
[24] J. del Bene, R. Ditchfield, and J. A. Pople, J. Chem. Phys. **55**, 2236 (1971).
[25] H. Nakatsuji and K. Hirao, J. Chem. Phys. **68**, 2053 (1978).
[26] H. Nakatsuji, Chem. Phys. Lett. **177**, 331 (1991).
[27] E. Runge and E. K. U. Gross, Phys. Rev. Lett. **52**, 997 (1984).
[28] E. K. U. Gross and W. Kohn, Phys. Rev. Lett. **55**, 2850 (1985).
[29] A. Dreuw and M. Head-Gordon, Chem. Rev. (Washington, D.C.) **105**, 4009 (2005).
[30] A. I. Krylov, Chem. Phys. Lett. **338**, 375 (2001).
[31] A. I. Krylov, Acc. Chem. Res. **39**, 83 (2006).
[32] L. V. Slipchenko and A. I. Krylov, J. Chem. Phys. **123**, 84107 (2005).
[33] Y. Shao, M. Head-Gordon, and A. I. Krylov, J. Chem. Phys. **118**, 4807 (2003).
[34] M. Seth and T. Ziegler, J. Chem. Phys. **123**, 144105 (2005).
[35] A. I. Krylov and C. D. Sherrill, J. Chem. Phys. **116**, 3194 (2002).
[36] A. I. Krylov, Chem. Phys. Lett. **350**, 522 (2001).
[37] J. S. Sears, C. D. Sherrill, and A. I. Krylov, J. Chem. Phys. **118**, 9084 (2003).
[38] D. Casanova and M. Head-Gordon, J. Chem. Phys. **129**, 064104 (2008).
[39] P. U. Manohar and A. I. Krylov, J. Chem. Phys. **129**, 194105 (2008).
[40] A. Golubeva, A. V. Nemukhin, L. Harding, S. J. Klippenstein, and A. I. Krylov, J. Phys. Chem. A **111**, 13264 (2007).
[41] L. V. Slipchenko and A. I. Krylov, J. Chem. Phys. **117**, 4694 (2002).
[42] A. I. Krylov, J. Phys. Chem. A **109**, 10638 (2005).
[43] K. Kowalski and P. Piecuch, J. Chem. Phys. **113**, 8490 (2000).
[44] J. B. Foresman, M. Head-Gordon, J. A. Pople, and M. J. Frisch, J. Phys. Chem. **96**, 135 (1992).
[45] T. Helgaker, P. Jørgensen, and J. Olsen, *Molecular Electronic Structure Theory* (Wiley, New York, 2000).
[46] Y. Shao, L. F. Molnar, Y. Jung, J. Kussmann, C. Ochsenfeld, S. Brown, A. T. B. Gilbert, L. V. Slipchenko, S. V. Levchenko, D. P. O'Neil, R. A. Distasio, Jr., R. C. Lochan, T. Wang, G. J. O. Beran, N. A. Besley, J. M. Herbert, C. Y. Lin, T. Van Voorhis, S. H. Chien, A. Sodt, R. P. Steele, V. A. Rassolov, P. Maslen, P. P. Korambath, R. D. Adamson, B. Austin, J. Baker, E. F. C. Bird, H. Daschel, R. J. Doerksen, A. Drew, B. D. Dunietz, A. D. Dutoi, T. R. Furlani, S. R. Gwaltney, A. Heyden, S. Hirata, C.-P. Hsu, G. S. Kedziora, R. Z. Khalliulin, P. Klunziger, A. M. Lee, W. Z. Liang, I. Lotan, N. Nair, B. Peters, E. I. Proynov, P. A. Pieniazek, Y. M. Rhee, J. Ritchie, E. Rosta, C. D. Sherrill, A. C. Simmonett, J. E. Subotnik, H. L. Woodcock III, W. Zhang, A. T. Bell, A. K. Chakraborty, D. M. Chipman, F. J. Keil, A. Warshel, W. J. Herhe, H. F. Schaefer III, J. Kong, A. I. Krylov, P. M. W. Gill, and M. Head-Gordon, Phys. Chem. Chem. Phys. **8**, 3172 (2006).
[47] A. I. Krylov, C. D. Sherrill, and M. Head-Gordon, J. Chem. Phys. **113**, 6509 (2000).
[48] M. W. Feyereisen, G. Fitzergald, and A. Komornicki, Chem. Phys. Lett. **208**, 359 (1993).

[49] O. Vahtras, J. Almof, and M. W. Feyereisen, Chem. Phys. Lett. **213**, 514 (1993).
[50] A. Komornicki and G. Fitzergald, J. Chem. Phys. **98**, 1399 (1993).
[51] D. E. Bernhold and R. J. Harrison, Chem. Phys. Lett. **250**, 477 (1996).
[52] C. Hättig and F. Weigend, J. Chem. Phys. **113**, 5154 (2000).
[53] C. Hättig and K. Hald, Phys. Chem. Chem. Phys. **4**, 2111 (2002).
[54] E. R. Davidson, J. Comput. Phys. **17**, 87 (1975).
[55] S. V. Levchenko, T. Wang, and A. I. Krylov, J. Chem. Phys. **122**, 224106 (2005).
[56] T. H. Dunning, J. Chem. Phys. **90**, 1007 (1989).
[57] P. C. Hariharan and J. A. Pople, Theor. Chim. Acta **28**, 213 (1973).
[58] See EPAPS Document No. E-JCPSA6-130-020904 for TMM diradical equilibrium geometries of the low-lying states obtained at SF-DFT(50/50)/6-31G* level and the B3LYP/cc-pVTZ equilibrium geometry of the $^5B_2$ state of DDMX tetraradical. For more information an EPAPS, see http://www.aip.org/epaps/numbering.html.
[59] H. Nakano, J. Chem. Phys. **99**, 7983 (1993).
[60] H. Nakano, Chem. Phys. Lett. **207**, 372 (1993).
[61] M. F. Guest, I. J. Bush, H. J. J. van Dam, P. Sherwood, J. M. H. Thomas, J. H. van Lenthe, R. W. A. Havenith, and J. Kendrick, Mol. Phys. **103**, 719 (2006).
[62] H.-J. Werner, P. J. Knowles, R. Lindh *et al.*, MOLPRO, Version 2008.1, a package of *ab initio* programs; see http://www.molpro.net.
[63] T. Yanai and G. K. C. Chan, J. Chem. Phys. **124**, 194106 (2006).
[64] C. D. Sherrill, Annu. Rep. Comp. Chem. **1**, 45 (2005).
[65] J. Barret and M. A. Malati, *Fundamentals of Inorganic Chemistry: An Introductory Text for Degree Course Studies* (Horwood Chemical Science, Chichester, 1998).
[66] P. Dowd, J. Am. Chem. Soc. **88**, 2587 (1966).
[67] R. J. Baseman, D. W. Pratt, M. Chow, and P. Dowd, J. Am. Chem. Soc. **98**, 5726 (1976).
[68] P. G. Wenthold, J. Hu, R. R. Squires, and W. C. Lineberger, J. Am. Chem. Soc. **118**, 475 (1996).
[69] C. J. Cramer and B. A. Smith, J. Phys. Chem. **100**, 9664 (1996).
[70] D. Feller, K. Tanaka, E. R. Davidson, and W. T. Borden, J. Am. Chem. Soc. **104**, 967 (1982).
[71] E. R. Davidson and W. T. Borden, J. Am. Chem. Soc. **99**, 2053 (1977).
[72] L. V. Slipchenko and A. I. Krylov, J. Chem. Phys. **118**, 6874 (2003).
[73] T. Wang and A. I. Krylov, J. Chem. Phys. **123**, 104304 (2005).
[74] L. V. Slipchenko, T. E. Munsch, P. G. Wenthold, and A. I. Krylov, Angew. Chem., Int. Ed. Engl. **43**, 742 (2004).
[75] M. Nooijen, K. R. Shamasundar, and D. Mukherjee, Mol. Phys. **103**, 2277 (2005).